Published in **Journal on Numerical Analysis** Vol. 52, No. 5, pp. 2315-2334, 2014

A locally modified parametric finite element method for interface problems

Stefan Frei * Thomas Richter †

We present a modified finite element method that is able to approximate interface problems with high accuracy. We consider interface problems, where the solution is continuous, its derivatives however may be discontinuous across interface curves within the domain. The proposed discretization is based on a local modification of the finite element basis which corresponds to a fitted finite element method. However, instead of moving mesh nodes, we resolve the interface locally by an adapted parametric approach. As all modifications are applied locally and in an implicit fashion, our scheme is very easy to implement and is well suited for time-dependent moving interface problems. We show optimal order of convergence for elliptic problems and further, we give a bound on the condition number of the system matrix. Both estimates do not depend on the interface location relative to the mesh.

1. Introduction

We propose an accurate, robust and easy to implement finite element method for interface problems, where the solution is continuous on a domain $\Omega \subset \mathbb{R}^2$, but its derivative may have a jump in normal direction over an interior interface $\Gamma := \partial\Omega_1 \cap \partial\Omega_2$ between two subdomains $\Omega_1 \subset \Omega$ and $\Omega_2 \subset \Omega$. Applications for such interface problems are multiphase flows or fluid-structure interactions. Both examples have in common, that the interface between the two phases is moving and may be difficult to capture due to small scale features. Here, we consider the simple Laplace equation

$$-\nabla \cdot (\kappa_i \nabla u) = f \text{ on } \Omega_i,\ i = 1, 2, \quad [u] = 0, \quad [\kappa \partial_n u] = 0 \text{ on } \Gamma, \tag{1}$$

where $\kappa_i > 0$ are diffusion parameters. By

$$[u](x) := \lim_{s \downarrow 0} u(x + sn) - \lim_{s \uparrow 0} u(x + sn), \quad x \in \Gamma,$$

we denote the jump of u at the interface Γ. The variational formulation of this interface problem is given by

$$u \in H_0^1(\Omega): \quad a(u, \phi) := \sum_{i=1}^{2} (\kappa_i \nabla u, \nabla \phi) = (f, \phi) \quad \forall \phi \in H_0^1(\Omega),$$

*Institute for Applied Mathematics, University of Heidelberg, stefan.frei@iwr.uni-heidelberg.de
†Institute for Applied Mathematics, University of Heidelberg, thomas.richter@iwr.uni-heidelberg.de

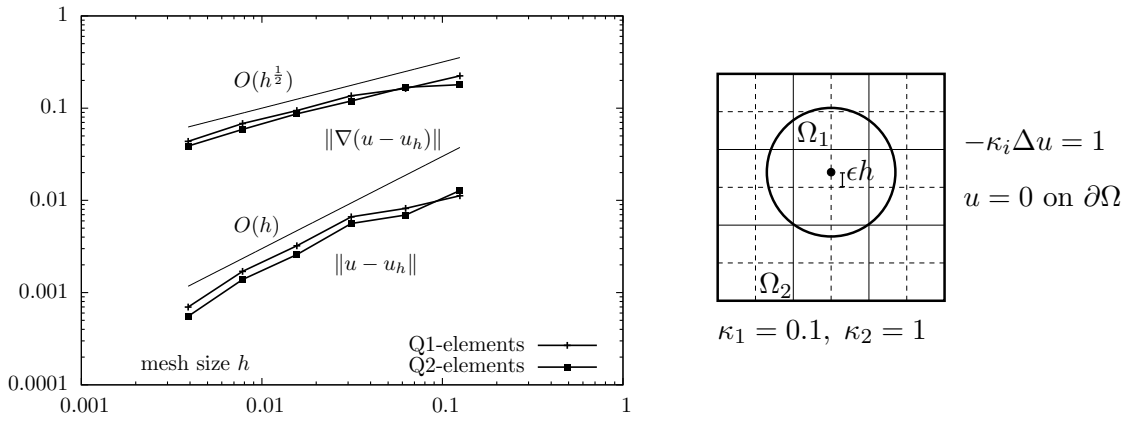

Figure 1: L^2- and H^1-error for a standard finite element simulation for a diffusion problem with a discontinuity in the diffusion coefficient. Configuration of the test-problem in the right sketch. Details on this problem are given in Section 11.

and existence of solutions can be shown by standard arguments. We assume, that the partitioning of Ω into Ω_1 and Ω_2 is non-overlapping $\Omega_1 \cap \Omega_2 = \emptyset$ and that both subdomains Ω_i $(i = 1, 2)$ have a boundary with sufficient regularity such that for smooth right hand sides it holds for the solution of (1), that

$$u \in H_0^1(\Omega) \cap H^{r+1}(\Omega_1 \cup \Omega_2),$$

for a given $r \in \mathbb{N}$, see Babuška [2].

Interface problems are elaborately discussed in literature. If the interface Γ cannot be resolved by the mesh, the overall error for a standard finite element ansatz will be bounded by

$$\|\nabla(u - u_h)\|_\Omega = \mathcal{O}(h^{1/2}),$$

independent of the polynomial degree r of the finite element space, see the early work of Babuška [2] or MacKinnon and Carey [16]. In Figure 1, we show the H^1 and L^2 errors for a simple interface problem with curved interface that is not resolved by the finite element mesh. Both linear and quadratic finite elements only give $\mathcal{O}(h^{1/2})$ accuracy in the H^1-seminorm and $\mathcal{O}(h)$ in the L^2-norm. This is due to the limited regularity of the solution across the interface.

It has been shown, that for interface problems with jumping coefficients causing weak discontinuities, optimal convergence can be recovered by a harmonic averaging of the diffusion constants [20, 19]. Such an averaging procedure has been applied to multiphase flows, it is however not suitable for problems, where two entirely different types of differential equations are coupled on the interface, as it is the case for fluid-structure interactions.

Given a fitted finite element configuration, the optimal order of convergence is guaranteed [2, 5, 10, 13, 21]. If the interface is moving, curved or has small scale features, the repeated generation of fitted finite element meshes can exceed the feasible effort. Further developments are based on local modifications of the finite element mesh, that only alter mesh elements close to the interface [8, 23]. By combining local mesh modifications close to the interface with an isoparametric approximation of curved interfaces, higher order approximation could be shown [12].

An alternative approach is based on unfitted finite elements, where the mesh is fixed and does not resolve the interface. Here, proper accuracy is gained by local modifications or enrichment of the

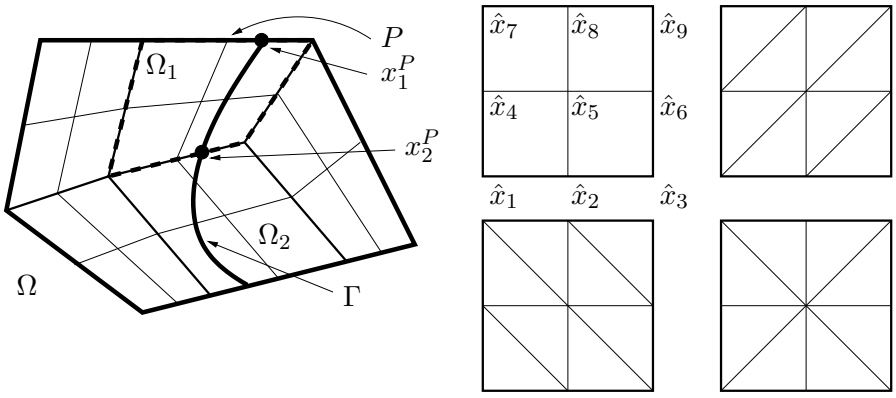

Figure 2: Left: triangulation Ω_h of a domain Ω, that split into Ω_1 and Ω_2 with interface Γ. The elements in Ω_h are arranged in a patched way. Patch P is cut by Γ at x_1^P and x_2^P. Right: subdivision of reference patches $\hat{P}_1, \hat{P}_2, \hat{P}_3, \hat{P}_4$ (top left to bottom right) into four quadrilaterals or eight triangles.

finite element basis. Prominent examples for these methods are the extended finite element method (XFEM) [17], the generalized finite element method [3] or the unfitted Nitsche method by Hansbo and Hansbo [14, 15], that casts the XFEM method into a new light. These enrichment methods are well analyzed and show the correct order of convergence. One drawback of these methods is a complicated structure that requires local modifications in the finite element spaces leading to variations in the connectivity of the system matrix and number of unknowns.

Here, we propose a finite element technique for interface problems that fits both into the context of fitted methods and modified finite element schemes. Our technique is equivalent to a fitted approach based on a mixed triangular-quadrilateral mesh. However, instead of resolving the interface by a motion or addition of mesh nodes, we locally adapt finite element basis functions in an implicit parametric way, such that weak discontinuities at the interface can be captured. This scheme requires neither an enrichment of the basis nor a modification of the mesh. The number of unknowns and also the connectivity pattern of the system matrix will not depend on the location of the interface.

The organization of this article is as follows: in Section 2 we describe the iso-parametric finite element approach used to resolve the interfaces and we give an optimal order a priori error analysis for the modified finite element method. In Section 6, we show, that the modified finite element method can be constructed such that the condition number of the system matrix is still bounded by $\mathcal{O}(h^{-2})$ and does not depend on the interface location. Section **??** gives some note on an efficient implementation of the required modifications in finite element codes. Finally, in Section 11 we show numerical results that demonstrate the accuracy and robustness of our proposed method. We conclude in Section 12.

2. Interface finite elements

Let Ω_h be a form and shape-regular triangulation of the domain $\Omega \subset \mathbb{R}^2$ into open quadrangles. The mesh Ω_h does not necessarily resolve the partitioning $\Omega = \Omega_1 \cup \Gamma \cup \Omega_2$ and the interface Γ can cut the elements $K \in \Omega_h$. We further assume, that the mesh Ω_h has a patch-hierarchy in such a way, that each four adjacent quads arise from uniform refinement of one common father-element, see Figure 2. Such a mesh-hierarchy is naturally given for finite element methods based on adaptive mesh refinement and also commonly used for error estimation methods [7] or projection based stabilization schemes [6].

The interface Γ may cut the patches in the following way:

1. Each (open) patch $P \in \Omega_h$ is either not cut $P \cap \Gamma = \emptyset$ or cut in exactly two points on its boundary: $P \cap \Gamma \neq \emptyset$ and $\partial P \cap \Gamma = \{x_1^P, x_2^P\}$.
2. If a patch is cut, the two cut-points x_1^P and x_2^P may not be inner points of the same edge.

In principle, these assumptions only rule out two possibilities: a patch may not be cut multiple times and the interface may not enter and leave the patch at the same edge. Both situations can be avoided by refinement of the underlying mesh. If the interface is matched by an edge, the patch is not considered cut.

2.1. Modification of the finite element space

We define the finite element trial space $V_h \subset H_0^1(\Omega)$ as iso-parametric space on the triangulation Ω_h:

$$V_h = \left\{ \phi \in C(\bar{\Omega}),\ \phi \circ T_P^{-1}\Big|_P \in \hat{Q} \text{ for all patches } P \in \Omega_h \right\},$$

where $T_P \in [\hat{Q}]^2$ is the mapping between the reference patch $\hat{P} = (0,1)^2$ and every patch $P \in \Omega_h$ such that

$$T_P(\hat{x}_i) = x_i^P, \quad i = 1, \dots, 9,$$

for the nine nodes $x_1^P, \dots, x_9^P$ in every patch, see Figure 2 (left). The reference space $\hat{Q}$ is a piecewise polynomial space of degree 1, that will depend on whether a patch P is cut by the interface or not. For patches $P \in \Omega_h$ not cut by the interface, we choose the standard space of piecewise bilinear functions:

$$\hat{Q} = \left\{ \phi \in C(\bar{P}),\ \phi\Big|_{K_i} \in \operatorname{span}\{1, x, y, xy\},\ K_1, \dots, K_4 \in P \right\}.$$

If a patch $P \in \Omega_h$ is cut by the interface, we divide the reference patch into eight triangles $T_1, \dots, T_8$ and define

$$\hat{Q}_{\text{mod}} = \left\{ \phi \in C(\bar{P}),\ \phi\Big|_{T_i} \in \operatorname{span}\{1, x, y\},\ T_1, \dots, T_8 \in P \right\}.$$

Depending on the position of the interface Γ in the patch P, three different reference configurations are considered, see the right sketch in Figure 2.

It is important to note, that the functions in $\hat{Q}$ and $\hat{Q}_{\text{mod}}$ are all piecewise linear on the edges ∂P, such that mixing different element types does not affect the continuity of the global finite element space. We denote by $\{\hat{\phi}^1, \dots, \hat{\phi}^9\}$ the standard Lagrange basis of $\hat{Q}$ or $\hat{Q}_{\text{mod}}$ with $\hat{\phi}^i(x_j) = \delta_{ij}$. The transformation T_P is given by

$$T_P(x) = \sum_{i=1}^{9} x_i^P \hat{\phi}_i(x).$$

Next, we present the subdivision of interface patches P into eight triangles each. We distinguish four different types of interface cuts, see Figure 3:

Configuration A The patch is cut at the interior of two opposite edges.

Configuration B The patch is cut at the interior of two adjacent edges.

Configuration C The patch is cut at the interior of one edge and in one node.

Configuration D The patch is cut in two opposite nodes.

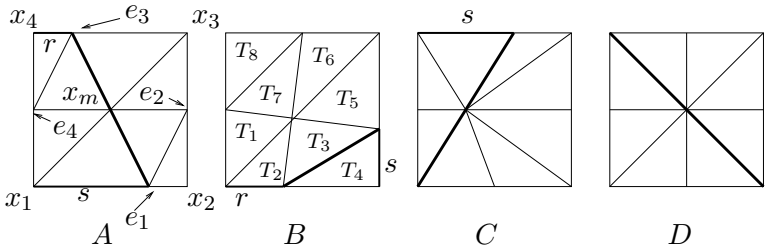

Figure 3: Different types of cut patches. The subdivision can be anisotropic with $r, s \in (0, 1)$ arbitrary.

Configurations A and B are based on the reference patches $\hat{P}_2$ and $\hat{P}_3$, configurations C and D use the reference patch $\hat{P}_4$, see Figure 2. By $e_i \in \mathbb{R}^2$, $i = 1, 2, 3, 4$ we denote the vertices on the edges, by $x_m \in \mathbb{R}^2$ the midpoint of the patch. The parameters $r, s \in (0, 1)$ describe the relative position of the intersection points with the interface on the outer edges.

If an edge is intersected by the interface we move the corresponding point e_i on this edge to the point of intersection. The position of the midpoint x_m depends on the specific configuration. For configuration A, B and D, we choose x_m as the intersection of the line connecting e_2 and e_4 with the line connecting e_1 and e_3. In configuration C, we use the intersection of the line connecting e_2 and e_4 with the line connecting x_1 and e_3.

Remark 3 *The finite element space V_h could be defined equivalently as a mixed linear-bilinear finite element space based on a mixed triangular-quadrilateral mesh. In our practical implementation, however, we use the patch grid Ω_h consisting of quadrilaterals only. The local degrees of freedom are incorporated implicitly by means of the local transformation T_P. Details on the implementation will be given in Section* **??**.

As the cut of the elements can be arbitrary with $r, s \to 0$ or $r, s \to 1$, the triangle's aspect ratio can be very large, considering $h \to 0$ it is not necessarily bounded. We can however guarantee, that the maximum angles in all triangles will be well bounded away from 180°:

Lemma 4 (Maximum angle condition) *All interior angles of the triangles shown in Figure 3 are bounded by* 144° *independent of $r, s \in (0, 1)$.*

Proof: All interior angles can be estimated by basic geometric analysis depending on the parameters $r, s \in (0, 1)$. We will show that in each triangle there is at least one angle larger than 36°. Hence, every angle will be bounded by 144°. This is in particular true for all triangles that are right angled.

Configuration A and B: We number the eight triangles of a patch by $T_1 ... T_8$ (cf. Figure 3). The two outer triangles T_4 and T_8 are right angled, such that $\alpha \leq 90°$ for all interior angles in T_4 and T_8. Furthermore, in configuration A the angles of T_1 at point e_4 and T_5 at point e_2 are right angled. For the angles in T_2 at e_1 and in T_6 at e_3 it holds

$$\cos(\alpha_A) = \pm \frac{(e_3 - e_1) \cdot (x_2 - x_1)}{|e_3 - e_1|\,|x_2 - x_1|} = \pm \frac{r - s}{\sqrt{1 + (r - s)^2}} \in \left(-\frac{1}{\sqrt{2}}, \frac{1}{\sqrt{2}} \right),$$

such that $\alpha_A \in (45°, 135°)$. In configuration B these four angles are given by

$$\cos(\alpha_B) = \pm \frac{(e_3 - e_1) \cdot (x_2 - x_1)}{|e_3 - e_1|\,|x_2 - x_1|} = \pm \frac{1/2 - r}{\sqrt{1 + (1/2 - r)^2}} \in \left(-\frac{1}{\sqrt{5}}, \frac{1}{\sqrt{5}} \right),$$

which means $\alpha_B \in (70°, 110°)$. Finally for configuration A and B it holds for the interior angles of T_3 and T_7 at x_m:

$$\cos(\alpha) = \pm \frac{(e_3 - e_1) \cdot (e_2 - e_4)}{|e_3 - e_1|\,|e_2 - e_4|}$$

Considering configuration A, it holds

$$\cos(\alpha_A) = \pm \frac{r-s}{\sqrt{1+(r-s)^2}} \in \left(-\frac{1}{\sqrt{2}}, \frac{1}{\sqrt{2}}\right) \quad \Rightarrow \quad \alpha_A \in (45°, 135°).$$

For configuration B, we get

$$\cos(\alpha_B) = \pm \frac{s-r}{\sqrt{1+\left(s-\frac{1}{2}\right)^2}\sqrt{1+\left(r-\frac{1}{2}\right)^2}} \in \left(-\frac{4}{5}, \frac{4}{5}\right) \quad \Rightarrow \quad \alpha_B \in (36°, 144°).$$

Configuration C: Here, the four triangle touching nodes e_2 and e_4 all have one right angle. It remains to estimate the interior angles at nodes e_1 and e_3. For these angles, it holds:

$$\cos(\alpha_C) = \pm \frac{\begin{pmatrix}1\\0\end{pmatrix} \cdot \begin{pmatrix}s\\1\end{pmatrix}}{\left|\begin{pmatrix}s\\1\end{pmatrix}\right|} = \pm \frac{s}{\sqrt{1+s^2}} \in \left(-\frac{1}{\sqrt{2}}, \frac{1}{\sqrt{2}}\right) \quad \Rightarrow \quad \alpha_C \in (45°, 135°).$$

Configuration D: Obviously, all triangles are right angled. □

4.1. A priori error analysis

We use the usual Lebesgue spaces $L^p(\Omega)$ and Sobolev spaces $H^k(\Omega)$ and their corresponding norms. For the $L^2(\Omega)$ norm, we will use the notation $\|\cdot\|_\Omega$ and sometimes skip the domain index if the context is clear.

The maximum angle conditions of Lemma 4 allows us to define robust Lagrangian interpolation operators $L_h : H^2(T) \cap C(\bar{T}) \to V_h$ with accurate error estimates

$$\|\nabla^k (v - L_h v)\|_T \leq c h_{T,\max}^{2-k} \|\nabla^2 v\|_T, \quad k = 0, 1, \tag{2}$$

with constants $c > 0$ and $h_{T,\max}$ is the maximum diameter of a triangle $T \in P$ (see e.g. [1]). The interpolation error estimates are robust with respect to the maximum diameter $h_{T,\max} \approx h_P$ that is of the same order as the diameter of the patches P. We do not get (and will not depend on) an optimal interpolation result with respect to the anisotropic triangles in terms of short edges $h_{T,\min} \ll h_{T,\max}$.

Theorem 5 (A priori estimate) *Let $\Omega \subset \mathbb{R}^2$ be a domain with convex polygonal boundary, split into $\Omega = \Omega_1 \cup \Gamma \cup \Omega_2$, where Γ is a smooth interface with C^2-parametrization. We assume that Γ divides Ω in such a way that the solution $u \in H_0^1(\Omega)$ satisfies the stability estimate*

$$u \in H_0^1(\Omega) \cap H^2(\Omega_1 \cup \Omega_2), \quad \|u\|_{H^2(\Omega_1 \cup \Omega_2)} \leq c_s \|f\|.$$

For the corresponding modified finite element solution $u_h \in V_h$ it holds

$$\|\nabla(u - u_h)\|_\Omega \leq Ch\|f\|, \quad \|u - u_h\|_\Omega \leq Ch^2\|f\|$$

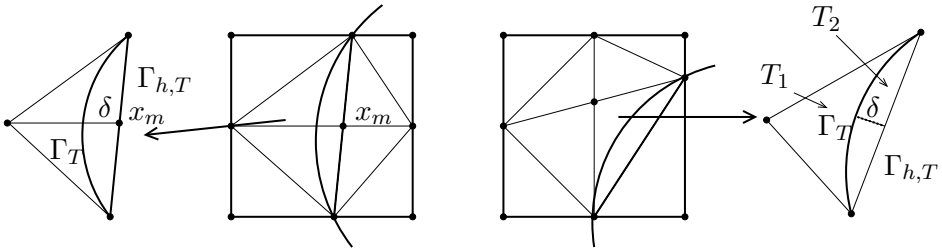

Figure 4: Two different patches and two triangles, that are affected by the interface-intersection. The modified finite element mesh does not resolve the interface.

PROOF: *(i)* As $V_h \subset H_0^1(\Omega)$, the usual best-approximation property holds for $I_h v \in V_h$:

$$\|\nabla(u - u_h)\| \leq C\|\nabla(u - I_h u)\|.$$

Further, for the solution $z \in H_0^1(\Omega) \cap H^2(\Omega_1 \cup \Omega_2)$ of the adjoint problem

$$z \in H_0^1(\Omega) : \; a(\phi, z) = (e_h, \phi)\|e_h\|^{-1} \quad \forall \phi \in H_0^1(\Omega),$$

it holds $z \in H_0^1(\Omega) \cap H^2(\Omega_1 \cup \Omega_2)$ with $\|z\|_{H^2(\Omega_1 \cup \Omega_2)} \leq c_s$. Using Galerkin orthogonality, the L^2-error can be estimated in the standard fashion

$$\|u - u_h\| \leq C\|\nabla(u - u_h)\| \, \|\nabla(z - I_h z)\| \leq C\|\nabla(u - I_h u)\| \, \|\nabla(z - I_h z)\|.$$

If the interface Γ can be resolved by the modified finite element scheme, the result follows using the interpolation estimates (2).

(ii) Next, we consider a general C^2-parameterized interface not matched by the triangulation. A similar argumentation can be found in [5]. By Γ_h, we denote the discrete approximation of the interface given by mesh lines and by Ω_h^1 and Ω_h^2 the subdomains separated by Γ_h. Further, let $S_i \subset \Omega_h$ $(i = 1, 2)$ be the set of elements T belonging to Ω_h^i that are affected by the interface

$$S_i = \left\{ T \in \Omega_h^i \,\middle|\, T \cap \Gamma \neq \emptyset \right\}$$

and $S_h = S_1 \cup S_2$ their union.

In Figure 4 we show two possible configurations for patches, that are cut by the interface. We will analyze the situation shown in the right sketch, the left one can be treated in the same way by combining the two triangles to one and replacing $I_h u$ in x_m by the mean value of the two adjacent vertices. This simplifies the analysis at the cost of a slightly less sharp estimate.

It holds with (2)

$$\|\nabla(u - I_h u)\|_\Omega^2 = \|\nabla(u - I_h u)\|_{\Omega \setminus S_h}^2 + \|\nabla(u - I_h u)\|_{S_h}^2 \tag{3}$$

$$\leq Ch^2 \|\nabla^2 u\|_{\Omega_1 \cup \Omega_2}^2 + \|\nabla(u - I_h u)\|_{S_h}^2, \tag{4}$$

where we used the standard interpolation estimate on $\Omega \setminus S_h$ and afterwards extended the domain to the complete domain Ω.

(iii) It remains to estimate the second term in (4). Let $\tilde{u}_i \in H^2(\Omega)$ (i=1,2) a continuous extension of $u \in H^2(\Omega_i)$ to the complete domain Ω. Such an extension exists, as the boundary Γ is smooth, see e.g. Wloka [22], and it holds:

$$\|\tilde{u}_i - u\|_{H^2(\Omega_i)} = 0, \quad \|\tilde{u}_i\|_{H^2(\Omega)} \leq C\|u\|_{H^2(\Omega_i)}, \quad i = 1, 2. \tag{5}$$

We will derive an estimate for $\|\nabla(u - I_h u)\|_{S_1}^2$. The corresponding estimate on S_2 follows analogously. It holds by adding and subtracting $\tilde{u}_1$

$$\|\nabla(u - I_h u)\|_{S_1} \leq \|\nabla(u - \tilde{u}_1)\|_{S_1} + \|\nabla(\tilde{u}_1 - I_h u)\|_{S_1} \tag{6}$$
$$= \|\nabla(u - \tilde{u}_1)\|_{S_1} + \|\nabla(\tilde{u}_1 - I_h \tilde{u}_1)\|_{S_1}, \tag{7}$$

since $I_h u = I_h \tilde{u}_1$ on S_1 for the nodal interpolant. The interpolation error can be estimated by (2), followed by a very rough enlargement from S_1 to Ω and by using the continuity of the extension (5):

$$\|\nabla(\tilde{u}_1 - I_h \tilde{u}_1)\|_{S_1} \leq Ch\|\nabla^2 \tilde{u}_1\|_{S_1} \leq Ch\|\nabla^2 \tilde{u}_1\|_{\Omega} \leq Ch\|\nabla^2 u\|_{\Omega_1}. \tag{8}$$

To treat the first term in (6), we will need some additional notation. Let $T \in S_1$ be a triangle cut by the interface. By $\Gamma_T = \Gamma \cap T$ we denote the curved interface and by $\Gamma_{h,T}$ the corresponding edge in the triangle (see Figure 4). Further, we split T into $T_1 = \Omega_1 \cap T$ and $T_2 = \Omega_2 \cap T$. As Γ_T has a C^2-parametrization, it holds for the distance δ between $\Gamma_{h,T}$ and Γ_h

$$\delta = \mathcal{O}(h^2), \quad |T| = \mathcal{O}(h^2), \quad |T_1| = \mathcal{O}(h^2), \quad |T_2| = \mathcal{O}(h^3).$$

A transformation argument in combination with a Poincaré like estimate on the reference element yield

$$\|v\|_{T_2}^2 \leq C\left(h^2\|v\|_{\Gamma_T}^2 + h^4\|\nabla v\|_{T_2}^2\right)$$

for $v \in H^1(T_2)$ (see e.g. [9, 11]). We apply this inequality to $v = \nabla(u - \tilde{u}_1)$ and get

$$\|\nabla(u - \tilde{u}_1)\|_{T_2}^2 \leq C\left(h^2\|\nabla(u - \tilde{u}_1)\|_{\Gamma_T}^2 + h^4\|u - \tilde{u}_1\|_{H^2(T_2)}^2\right), \tag{9}$$

where the trace of (the discontinuous function) ∇u on Γ_T is the trace as seen from T_2. As $u = \tilde{u}_1$ on T_1, we can replace the domain T_2 by T on both sides of (9). Summation over $T \in S_1$ yields

$$\|\nabla(u - \tilde{u}_1)\|_{S_1}^2 \leq C\left(h^2\|\nabla(u - \tilde{u}_1)\|_{\Gamma}^2 + h^4\|u - \tilde{u}_1\|_{H^2(S_1)}^2\right). \tag{10}$$

For the boundary term on the right-hand side, we apply the (global) trace inequality and use the continuity of the extension (5)

$$\|\nabla(u - \tilde{u}_1)\|_{\Gamma}^2 \leq \|\nabla u\|_{\Gamma}^2 + \|\nabla \tilde{u}_1\|_{\Gamma}^2 \leq C\|u\|_{H^2(\Omega_1 \cup \Omega_2)}^2. \tag{11}$$

Finally, by combining (6) to (11) and using the analogous estimate on S_2 it follows, that

$$\|\nabla(u - I_h u)\|_{S_h} \leq Ch\|u\|_{H^2(\Omega_1 \cup \Omega_2)}.$$

□

6. Condition number analysis

The modified finite element ansatz described above has one serious drawback. For certain anisotropies (e.g. $s, r \to 0$) the condition number of the stiffness matrix is not bounded. To illustrate this, we consider an interface problem where Ω_1 is a circle inside the unit square Ω (see Figure 5 right sketch). To study the sensitivity with respect to anisotropies, we move the circle in vertical direction by ϵ. We will give further details on this example in Section 11. In Figure 5 left sketch, we show how

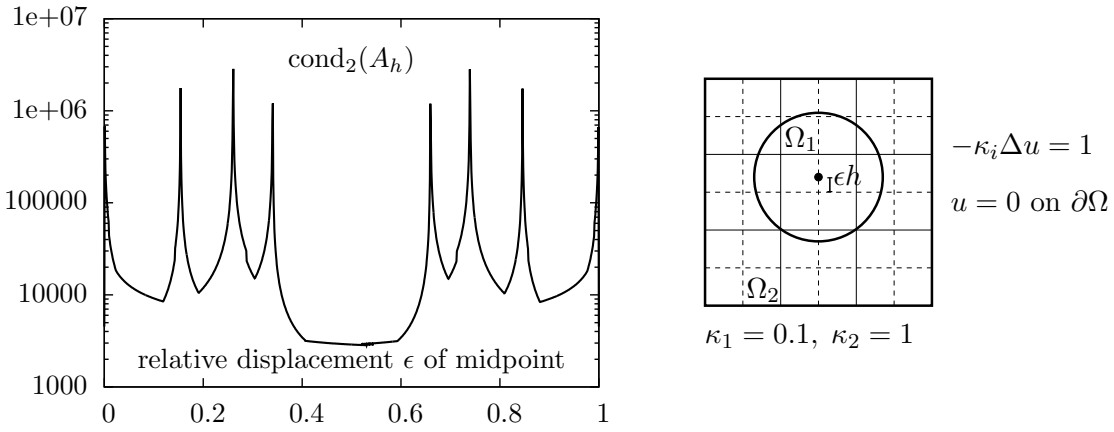

Figure 5: Condition number of the system matrix $\mathrm{cond}_2(A_h)$ depending on the displacement of the circle Ω_1.

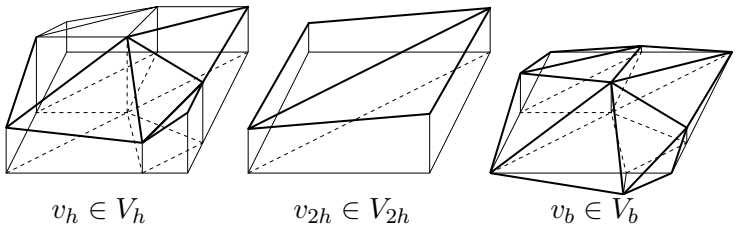

Figure 6: Example for a hierarchical splitting of a function $v_h \in V_h$ into coarse mesh part $v_{2h} \in V_{2h}$ and fine mesh fluctuation $v_b \in V_b$.

the condition number changes for different ϵ. For $\epsilon \to 0$, the condition number increases with order $\mathcal{O}(1/\epsilon)$.

In this section, we will present a scaled hierarchical finite element basis for the space V_h, that will yield system matrices A_h that satisfy the usual bound $\mathrm{cond}_2(A_h) = \mathcal{O}(h^{-2})$ with a constant that does not depend on the position of the interface Γ relative to the mesh elements.

We split the finite element space V_h in a hierarchical manner

$$V_h = V_{2h} + V_b, \quad N := \dim(V_h) = \dim(V_{2h}) + \dim(V_b) =: N_{2h} + N_b.$$

The space V_{2h} is the standard space of piecewise bilinear or linear functions on the patches $P \in \Omega_h$ equipped with the usual nodal Lagrange basis $V_{2h} = \mathrm{span}\{\phi_{2h}^1, \ldots, \phi_{2h}^{N_{2h}}\}$. Therefore, patches cut by the interface are split into two triangles.

The space $V_b = V_h \setminus V_{2h}$ collects all functions, that enrich V_{2h} to V_h. These functions are defined piecewise on $T_1, \ldots, T_8$ in the remaining 5 degrees of freedom, see Figure 6 for an example. The basis is denoted by $V_b = \mathrm{span}\{\phi_b^1, \ldots, \phi_b^{N_b}\}$. The finite element space V_{2h} is fully isotropic and standard analysis holds. Functions in V_{2h} do not resolve the interface, while the basis functions $\phi_b^i \in V_b$ will depend on the interface location if $\Gamma \subset \mathrm{supp}\ \phi_b^i$.

For a function $v_h \in V_h$ we use the (unique) splitting

$$v_h = \sum_i \mathbf{v}_h^i \phi_h^i = \sum_{i=1}^{N_{2h}} \mathbf{v}_{2h}^i \phi_{2h}^i + \sum_{i=1}^{N_b} \mathbf{v}_b^i \phi_b^i = v_{2h} + v_b \in V_{2h} + V_b.$$

We use the notation $\mathbf{v}_h^i, \mathbf{v}_{2h}^i$ and $\mathbf{v}_b^i$ to indicate the degrees of freedom in the spaces V_h, V_{2h} and V_b and introduce the vectors $\mathbf{v}_h, \mathbf{v}_{2h}$ and $\mathbf{v}_b$ defined by these components. For this splitting it holds:

Lemma 7 (Hierarchical finite element spaces) *For every $v_h = v_{2h} + v_b \in V_h$ it holds*

$$(i) \quad \|\nabla v_h\|^2 \leq 2\|\nabla v_{2h}\|^2 + 2\|\nabla v_b\|^2,$$

and further

$$(ii) \quad \|\nabla v_{2h}\|^2 + \|\nabla v_b\|^2 \leq C\|\nabla v_h\|^2,$$

with a constant $C > 0$.

Proof: The first inequality follows by $v_h = v_{2h} + v_b$. For deriving the second inequality, we need to exploit the hierarchical setup of the finite element spaces. First, by $i_{2h} : V_h \to V_{2h}$ we denote the nodal Lagrange interpolant into the coarse finite element space. Stability of this (discrete) interpolation gives the first half of the result

$$\|\nabla v_{2h}\| = \|\nabla i_{2h} v_h\| \leq C\|\nabla v_h\|.$$

By using the reverse triangle inequality, we get (ii)

$$\|\nabla v_b\| \leq \|\nabla(v_b + v_{2h})\| + \|\nabla v_{2h}\| \leq (1 + C)\|\nabla v_h\|$$

□

The following analysis, will be based on two essential assumptions for the test-functions of the spaces V_{2h} and V_b:

Assumption 7.1 (Finite Element Basis) *There exists a constant $C > 0$ independent of h and the interface location, such that it holds for every basis function*

$$C^{-1} \leq \|\nabla \phi_h^i\| \leq C, \quad i = 1, \ldots, N_b. \tag{12}$$

Further, there exists a constant $C > 0$ independent of h and the interface location, such that for all $v_b \in V_b$ it holds

$$|\mathbf{v}_b^i| \leq C\|\nabla v_b\|_{\mathcal{N}_i}, \quad i = 1, \ldots, N_b, \tag{13}$$

where by $\mathcal{N}_i = \{K \in \Omega_h,\ x_i \in \bar{K}\}$ we denote the neighborhood of all elements involving the Lagrange point x_i.

Both assumption hold true for standard finite element spaces on shape- and form-regular finite element meshes and can be shown by using inverse estimates. Assumption (12) is fulfilled after an appropiate scaling of the basis functions. Details as well as the very technical proof of (13) for the modified hierarchical finite element spaces will be given in the Appendix.

Next, we show two estimates for the large and small eigenvalues. These two results will be combined in Theorem 10 to show a bound for the condition number of the system matrix. The proofs follow the ideas of Bank and Scott [4].

Lemma 8 (Large eigenvalues) *There exists a constant $C > 0$ independent of the interface location, such that it holds:*

$$\mathbf{v}_h^T \mathbf{A}_h \mathbf{v}_h = a(v_h, v_h) \leq C\mathbf{v}_h^T \mathbf{v}_h \quad \forall v_h \in V_h.$$

PROOF: It holds

$$a(v_h, v_h) \leq C\|\nabla v_h\|^2 = C \sum_{P\in\Omega_h} \|\nabla v_h\|_P^2 = C \sum_{P\in\Omega_h} \left\| \sum_{x_i\in P} \mathbf{v}_h^i \nabla \phi_h^i \right\|^2$$

As only a finite number of basis functions have their support in P it holds

$$a(v_h, v_h) \leq C \sum_{P\in\Omega_h} \sum_{x_i\in P} |\mathbf{v}_h^i|^2 \|\nabla \phi_h^i\|_P^2$$

Using Assumption (12), it follows, that

$$a(v_h, v_h) \leq C \sum_{i=1}^{N} |\mathbf{v}_h^i|^2 = C\mathbf{v}_h^T \mathbf{v}_h.$$

where again we used, that every node x_i is part of only a limited number of patches. □

Next, we show an estimate for the small eigenvalues

Lemma 9 (Small eigenvalues) *There exists a function $C > 0$ independent on the interface location, such that it holds*

$$\mathbf{v}_h^T \mathbf{A}_h \mathbf{v}_h = a(v_h, v_h) \geq Ch^2 \mathbf{v}_h^T \mathbf{v}_h \quad \forall v_h \in V_h.$$

PROOF: Let $v_h = v_{2h} + v_b$. First, we will show the result separately for $v_{2h} \in V_{2h}$ and $v_b \in V_b$.

(i) We start with functions $v_{2h} \in V_{2h}$. Let $v_{2h} = \sum_{i=1}^{N_{2h}} \mathbf{v}_{2h}^i \phi_{2h}^i \in V_{2h}$:

$$\mathbf{v}_{2h}^T \mathbf{v}_{2h} = \sum_{i=1}^{N_{2h}} (\mathbf{v}_{2h}^i)^2 \leq \sum_{P\in\Omega_{2h}} \sum_{x_i\in P} (\mathbf{v}_{2h}^i)^2.$$

On a patch $P \in \Omega_{2h}$ it follows for $v_{2h} \in V_{2h}$ by using an inverse estimate for the standard nodal Lagrange basis

$$\sum_{x_i\in P} (\mathbf{v}_{2h}^i)^2 \leq C\|v_{2h}\|_{L^\infty(P)}^2 \leq Ch^{-2}\|v_{2h}\|_{L^2(P)}^2$$

Then by Poincaré's inequality on Ω, it finally holds

$$\mathbf{v}_{2h}^T \mathbf{v}_{2h} \leq Ch^{-2} \sum_{P\in\Omega_h} \|v_{2h}\|_{L^2(P)}^2 \leq Ch^{-2}\|v_{2h}\|^2 \leq Ch^{-2}\|\nabla v_{2h}\|^2. \tag{14}$$

(ii) Next, we treat the case $v_b \in V_b$. By using Assumption (13) we immediately get

$$\mathbf{v}_b^T \mathbf{v}_b = \sum_{i=1}^{N_b} (\mathbf{v}_b^i)^2 \leq C \sum_{i=1}^{N_b} \|\nabla v_b\|_{\mathcal{N}_i}^2 \leq C\|\nabla v_b\|^2, \tag{15}$$

where the constant C depends on the overlap of elements in the neighborhoods $\mathcal{N}_i$. The result follows, as $h^{-2} \geq 1$ for $h < 1$.

(iii) We combine these two results. By Lemma 7 it holds

$$\begin{aligned} \mathbf{v}_h^T \mathbf{A}_h \mathbf{v}_h = a(v_h, v_h) \geq C\|\nabla v_h\|^2 &\geq C\|\nabla v_{2h}\|^2 + C\|\nabla v_b\|^2 \\ &\geq C\left(a(v_{2h}, v_{2h}) + a(v_b, v_b)\right) \end{aligned}$$

Hence, using (14) and (15)

$$\mathbf{v}_h^T \mathbf{A}_h \mathbf{v}_h \geq Ch^2 \left(\mathbf{v}_{2h}^T \mathbf{v}_{2h} + \mathbf{v}_b^T \mathbf{v}_b \right) = Ch^2 \mathbf{v}_h^T \mathbf{v}_h.$$

□

Combining Lemma 8 and 9, we get an estimate for the condition number:

Theorem 10 (Condition number) *Under Assumption 7.1 it holds for the condition number*

$$\mathrm{cond}_2(\mathbf{A}) \leq Ch^{-2},$$

with a constant $C > 0$ not depending on the interface location.

11. Numerical examples

In this section, we design three different test-cases to validate the modified finite element technique introduced in Section 2. We will include all different types of interface cuts (configurations A to D) with arbitrary anisotropies including $r, s \to 0$ or 1.

11.1. Example 1: circular interface

This first example has already been considered to discuss the interface approximation in Section 2 and the dependency of the condition number on the interface in Section 6, see Figure 1 for a sketch of the configuration. The unit square $\Omega = (-1, 1)^2$ is split into a ball $\Omega_1 = B_R(x_m)$, where $R = 0.5$ and $x_m = (0, \epsilon h)$ for an $\epsilon \in [0, 1]$ and $\Omega_1 = \Omega \setminus \bar{\Omega}_2$. As diffusion parameters we choose $\kappa_1 = 0.1$ and $\kappa_2 = 1$ within the inner ball. We choose the analytical solution

$$u(x) = \begin{cases} -2\kappa_2 \|x - x_m\|^4, & x \in \Omega_2, \\ -\kappa_1 \|x - x_m\|^2 + \frac{1}{4}\kappa_1 - \frac{1}{8}\kappa_2 & x \in \Omega_1, \end{cases}$$

to define right hand side $f_i := -\kappa_i \Delta u$ and Dirichlet boundary data. After some steps of global refinement this simple example includes configurations A to C. In Figure 7, we plot the the H^1- and L^2-norm errors obtained on several levels of global mesh refinement. According to Theorem 5 of Section 4.1, we observe linear convergence in the H^1-norm and quadratic convergence in the L^2-norm. For comparison, Figure 1 shows the corresponding results using the standard non-fitting basis functions. A sketch of the solution is given in the right side of Figure 7.

Next, in Figure 8, we show a study of the condition number's dependency on the parameter $\epsilon \in [0, 1]$ used to shift the midpoint of the circle $x_m = (0, \epsilon h)$. The scaled hierarchical ansatz space shows optimal behavior $\mathcal{O}(h^{-2})$ with regard to mesh size h and no dependency on the shift ϵ, while the standard approach shows very large conditions numbers with $\mathrm{cond}_2(A_h) \to \infty$ for $\epsilon \to 0$ and $\epsilon \to 1$.

11.2. Example 2: horizontal cuts

To study the different cuts of interface patches in more detail, let us next consider that $\Omega = (-1, 1)^2$ is cut horizontally into

$$\Omega_1(\epsilon) = \left\{ x \in \Omega \,\middle|\, x_2 < \epsilon h \right\}, \quad \Omega_2(\epsilon) = \left\{ x \in \Omega \,\middle|\, x_2 > \epsilon h \right\}.$$

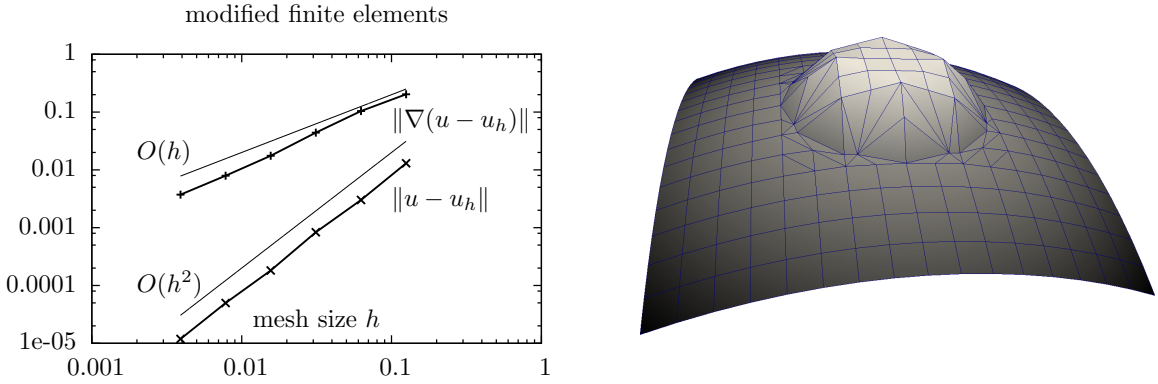

Figure 7: Example 1: H^1- and L^2-Error under mesh refinement. Right: sketch of the solution.

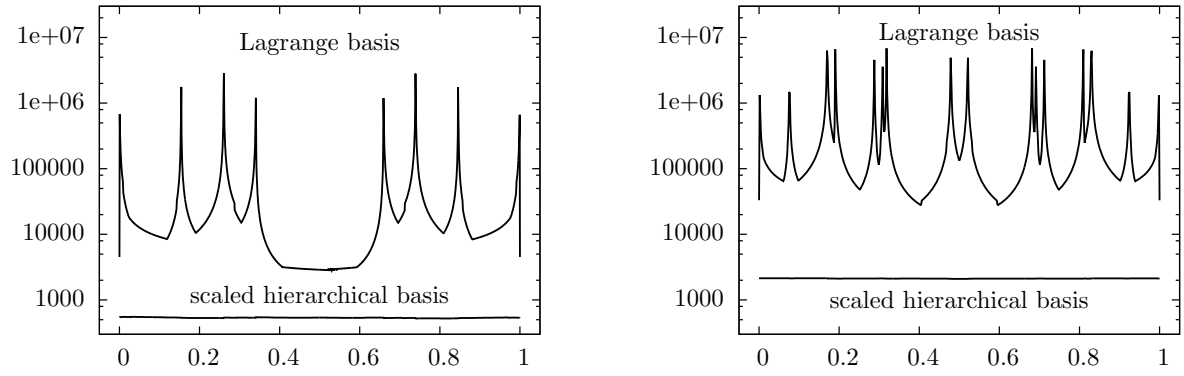

Figure 8: Example 1: condition number of the system matrix depending on the displacement of the circle Ω_1 by ϵh for $\epsilon \in [0,1]$. Standard Lagrange basis versus the scaled hierarchical basis introduced in Section 6. Left $h = 1/16$, right $h = 1/32$.

By varying $\epsilon \in [0,1]$ the interface patches of a Cartesian mesh will be split into rectangulars with vertical edge lengths ϵh and $(1-\epsilon)h$, $0 < \epsilon < 1$. We choose right hand side $f = -\kappa_i \Delta u$ and Dirichlet data according to the solution

$$u(x) = \begin{cases} \frac{\kappa_2}{\kappa_1}(x_2 - \epsilon h) - (x_2 - \epsilon h)^2 & x \in \Omega_1 \\ (x_2 - \epsilon h) + (x_2 - \epsilon h)^2 & x \in \Omega_2. \end{cases} \tag{16}$$

In Figure 9, we plot L^2-norm and H^1-norm error for $0 \le \epsilon \le 1$ on meshes with patch size $h = 1/16$ and $h = 1/32$. Both errors clearly depend on the position ϵ of the cut. As one would expect, we get the smallest errors for $\epsilon = 0$, $\epsilon = \frac{1}{2}$ and $\epsilon = 1$, where the mesh is perfectly uniform and resolves the cut. The largest error given for $\epsilon \to 0$ and $\epsilon \to 1$, where the anisotropy of the interface patches is maximal. Nevertheless, we see that the error remains bounded for all $\epsilon \in [0,1]$. The variations get smaller on the finer mesh.

To explain these error variations we briefly analyze the interpolation error. The mesh consists of h^{-2} patches. Only h^{-1} patches are affected by the interface. These are cut into $2h^{-1}$ quads of size $h/2 \times \epsilon h$ and $2h^{-1}$ quads of size $h/2 \times (1-\epsilon)h$. The remaining $4h^{-2} - 4h^{-1}$ quads all have the size $h/2 \times h/2$. As the interface is a horizontal line, the modified mesh is still Cartesian and due to superconvergence

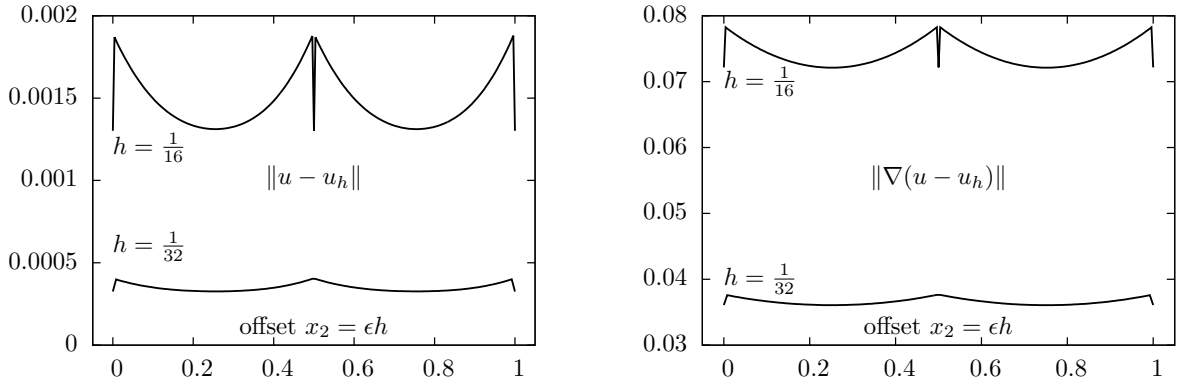

Figure 9: Example 2: L^2- and H^1-norm error depending on a vertical offset $x_2 = \epsilon h$ of the interface.

Table 1: Example 2: maximum and minimum error under vertical displacement ϵh of the interface line. Comparison of errors with the predicted error variation.

	H^1-error		L^2-error	
	$h = 1/16$	$h = 1/32$	$h = 1/16$	$h = 1/32$
Worst case ($\epsilon = 10^{-6}h$)	$7.864 \cdot 10^{-2}$	$3.774 \cdot 10^{-2}$	$1.904 \cdot 10^{-3}$	$4.077 \cdot 10^{-4}$
Best case ($\epsilon = h$)	$7.217 \cdot 10^{-2}$	$3.608 \cdot 10^{-2}$	$1.302 \cdot 10^{-3}$	$3.255 \cdot 10^{-4}$
Prediction	1.090	1.046	1.392	1.212
Variation	1.090	1.046	1.462	1.252

effects the errors we observe are essentially the interpolation errors $\|u - I_h u\|$. The solution u only depends on x_2, see (16). For the L^2-norm, it holds on an element K of size $h_1 \times h_2$:

$$\|u - I_h u\|_K^2 \leq c h_2^4 \|\partial_{22} u\|_K^2 \approx c h_1 h_2^5.$$

summed over all elements $K \in \Omega_h$, we get the interpolation bound

$$\|u - L_h u\|_\Omega^2 \approx \left(4h^{-2} - 4h^{-1}\right) \frac{h^6}{64} + 2h^{-1}\epsilon^5 \frac{h^6}{2} + 2h^{-1}(1-\epsilon)^5 \frac{h^6}{2}.$$

In the best case, for $\epsilon = \frac{1}{2}$, it holds

$$\|u - I_h u\|_\Omega^2 \approx \frac{h^4}{16},$$

while in the worst case for $\epsilon \to 0$ or $\epsilon \to 1$ we get

$$\|u - I_h u\|_\Omega^2 \approx \frac{h^4}{16}(1 + 15h)$$

Hence, the L^2-norm error varies by a factor of $\sqrt{1+15h}$ which relates to approximately $\sqrt{2} \approx 1.4$ for $h = 1/16$ and $\sqrt{3/2} \approx 1.2$ for $h = 1/32$. For the H^1-norm a similar analysis leads to a variation factor of $\sqrt{1+3h}$. In Table 11.2, we gather variation factors between maximum and minimum L^2- and H^1-norm on both meshes and find very good agreement to the prediction.

11.3. Example 3: tilted interface line

Next, we consider two subdomains that are separated by a straight interface line through the origin, which might be horizontal ($\alpha = 0$), vertical ($\alpha = \pi/2$) or inclined ($0 < \alpha < \pi/2$ or $\pi/2 < \alpha < \pi$). The

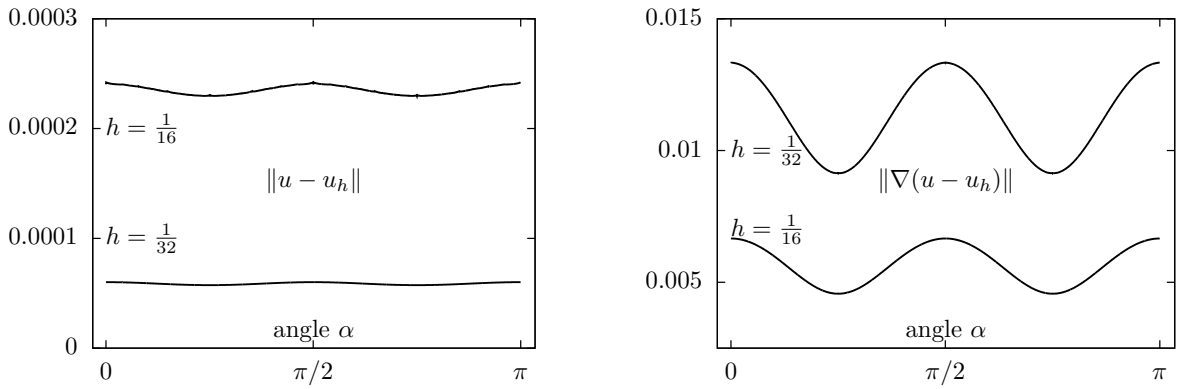

Figure 10: Example 3: L^2- and H^1-norm error for a line cutting at different angles $\alpha \in [0, \pi]$.

interface Γ_i is defined by the relation $\cos(\alpha)x_2 = \sin(\alpha)x_1$ given the partitioning:

$$\Omega_1^\alpha = \left\{x \in \Omega \,\middle|\, \cos(\alpha)x_2 < \sin(\alpha)x_1\right\},$$
$$\Omega_2^\alpha = \left\{x \in \Omega \,\middle|\, \cos(\alpha)x_2 > \sin(\alpha)x_1\right\}.$$

We choose right hand side $f = -\kappa_i \Delta u$ and Dirichlet data according to the given exact solution:

$$u(x) = \begin{cases} \sin\left(\frac{\kappa_2}{\kappa_1}(\cos(\alpha)x_2 - \sin(\alpha)x_1)\right), & x \in \Omega_1 \\ \sin\left(\cos(\alpha)x_2 - \sin(\alpha)x_1\right) & x \in \Omega_2. \end{cases}$$

In Figure 10 we plot the L^2- and H^1-norm error for angles $\alpha = 0...\pi$ and two different refinement levels ($h = 1/16$ and $h = 1/32$). In the case $\alpha = \pi/2$ all the interface patches are of type D, while in the other cases types A to C appear with all kinds of anisotropies inside. Again, we observe linear convergence for the H^1-norm error and quadratic convergence in the L^2-norm. The error varies up to a factor of approximately $\sqrt{2}$ in the case of the H^1-norm and about 1.05 in the L^2-norm which can be explained similarly to the case of horizontal cuts. We emphasize that these variations are again bounded for all $\alpha \in [0, \pi]$.

12. Conclusion

We have presented a new modified finite element method for interface problems. Discontinuities in the normal derivative of the solution are captured by a parametric finite element approach, that is based on a patchwise subdivision of the finite element mesh into triangles. Instead of moving mesh nodes, the interface capturing is realized by using a parametric finite element setup.

Further, we have shown optimal approximation order, that does not depend on the interface location within the finite element mesh. And finally, by constructing the finite element spaces in a hierarchical way, the resulting system matrices have a condition number that satisfies the usual bound $\mathcal{O}(h^{-2})$ independent of the interface location.

In upcoming research, this modified finite element method will be applied to problems with moving interfaces, as they appear in fixed-mesh formulations of fluid-structure interaction problems, see e.g. [18]
.

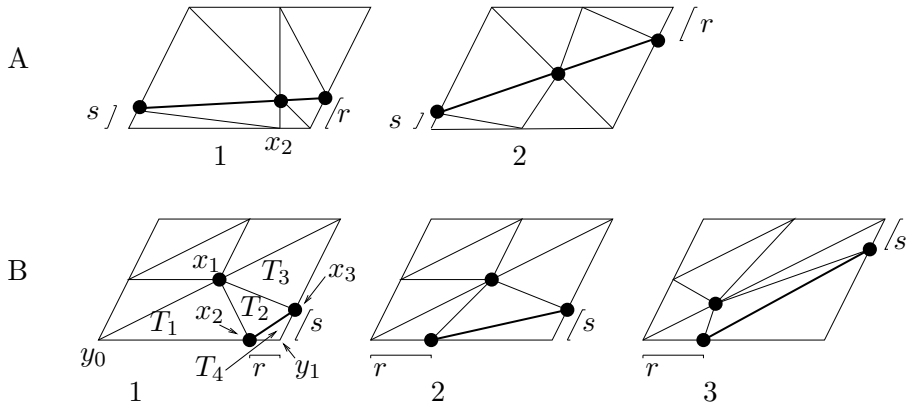

Figure 11: Configuration of the hierarchical basis functions V_b for the different patch-types. In each sketch, we consider the case $r \to 0$ or $s \to 0$ or both.

A. Setup of the Finite Element Basis

In this appendix, we give details on Assumption 7.1, required for proving the boundedness of the condition number. In this assumption, we call for two conditions on the basis functions. First, every basis function $\phi_i \in V_h$ should be bounded by

$$C^{-1} \leq \|\nabla \phi_h^i\|^2 \leq C, \tag{17}$$

with a constant $C > 0$ (independent of h and the interface location). Second, there should exist a constant $C > 0$, such that for each degree of freedom $i \in [1, N_b]$ of the "add-on" space V_b it holds:

$$(\mathbf{v}_b^i)^2 \leq C \|\nabla v_b\|_{\mathcal{N}_i}^2 \quad \forall v_b \in V_b,$$

where by $\mathcal{N}_i$ we denote all elements of Ω_h that have x_i as node.

These two assumptions hold true for standard finite elements on form- and shape-regular meshes and can be easily derived using inverse estimates. For the modified finite element ansatz defined in Section 2 the proof of these assumptions is technical. In order to define a hierarchical ansatz space, we have to modify some of the basic triangles. In Figure 11 we show the cases A and B, case C is treated similarly. In contrast to Section 2, the midpoint is moved along one of the diagonal lines only. Then, we define the space V_{2h} as the space of piecewise linear functions on the two large triangles. In order to guarantee a maximum angle condition in case A.1, we must also move the outer node x_2 belonging to the space V_b.

Each of the two large triangles forming the patch P is split into four subtriangles and the space V_{2h} is enriched to V_h by the Lagrangian basis with respect to the subtriangles on the remaining nodes. In Figure 12, we illustrate two hierarchical basis functions from V_{2h} and two basis functions from V_b for an isotropic element.

Next, we give details for the derivation of Assumption 7.1 for some typical configurations.

A.1. Assumption 1 - scaling of the basis functions

We only have to consider the basis functions $\phi_b^i \in V_b$, as this assumption holds for the standard space V_{2h}. By $\tilde{\phi}_b^i$ we denote the standard nodal Lagrange functions satisfying $\tilde{\phi}_b^i(x_j) = \delta_{ij}$, where x_i is one

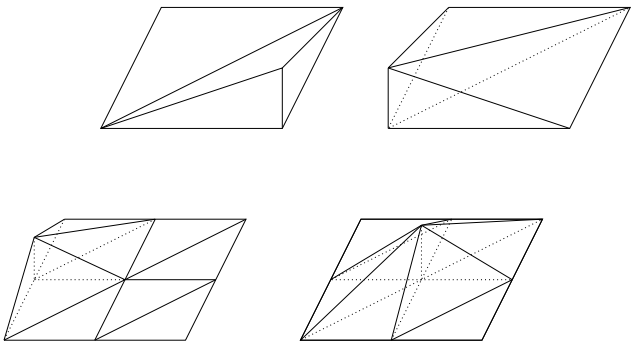

Figure 12: Above: Two basis functions $\phi_i^{2h} \in V_{2h}$, below two basis functions $\phi_i^b \in V_b$

of the Lagrange points shown in Figure 11. We will derive the proper scaling factor for configuration B.1 in Figure 11, where r, s are small and where $r, s \to 0$ is possible. It holds for the gradients of the three test-functions in the four different triangles:

$$\begin{aligned}
&\|\nabla\tilde{\phi}_1\|^2_{T_1} = \mathcal{O}(1) && \|\nabla\tilde{\phi}_1\|^2_{T_2} = \mathcal{O}(\sqrt{r^2+s^2}) && \|\nabla\tilde{\phi}_1\|^2_{T_3} = \mathcal{O}(1)\\
&\|\nabla\tilde{\phi}_2\|^2_{T_1} = \mathcal{O}(1) && \|\nabla\tilde{\phi}_2\|^2_{T_2} = \mathcal{O}\left(\min\left\{\frac{1}{r},\frac{1}{s}\right\}\right) && \|\nabla\tilde{\phi}_2\|^2_{T_4} = \mathcal{O}\left(\frac{s}{r}\right)\\
&\|\nabla\tilde{\phi}_3\|^2_{T_2} = \mathcal{O}\left(\min\left\{\frac{1}{r},\frac{1}{s}\right\}\right) && \|\nabla\tilde{\phi}_3\|^2_{T_3} = \mathcal{O}(1) && \|\nabla\tilde{\phi}_3\|^2_{T_4} = \mathcal{O}\left(\frac{r}{s}\right).
\end{aligned}$$

Hereby, we can read out the proper scaling factor for every test-function. We define

$$\tau_1 = 1, \quad \tau_2 = \sqrt{\min\left\{\max\{r,s\},\frac{r}{s}\right\}}, \quad \tau_3 = \sqrt{\min\left\{\max\{r,s\},\frac{s}{r}\right\}} \tag{18}$$

and set

$$\phi_i := \tau_i\tilde{\phi}_i, \quad i = 1...3 \tag{19}$$

such that $\|\nabla\phi_i\| = \mathcal{O}(1)$ for all $r, s \in [0,1]$.

Remark B (Estimation of the scaling factors) *The scaling factors for the remaining cases can be estimated in a similar way. However, in a practical implementation, one can use the hierarchical Lagrangian basis $\tilde{\phi}_i$ to assemble the system matrix $\tilde{A}_h$ and apply a simple row- and column-wise scaling with the diagonal elements:*

$$\tilde{a}_{ij} = (\nabla\tilde{\phi}_j, \nabla\tilde{\phi}_i), \quad a_{ij} := \frac{\tilde{a}_{ij}}{\sqrt{\tilde{a}_{ii}\tilde{a}_{jj}}},$$

which yields directly (cf. Section **??***)*

$$\|\nabla\phi_h^i\|^2 = a_{ii} = \frac{\tilde{a}_{ii}}{\tilde{a}_{ii}} = 1.$$

B.1. Assumption 2

Next, we must show the existence of a constant $C > 0$, such that for all $i \in [1, N_b]$ it holds

$$(\mathbf{v}_b^i)^2 \le C\|\nabla v_b\|^2_{\mathcal{N}_i} \quad \forall v_b \in V_b. \tag{20}$$

It is sufficient to show, that for each Lagrange point x_i, it holds

$$(\mathbf{v}_b^i)^2 \leq C\|\nabla v_b\|_T^2 \quad \forall v_b \in V_b, \tag{21}$$

for at least one triangle $T \subset \mathcal{N}_i$. Due to the form and shape-regularity of the patch mesh, it suffices to show (21) on the corresponding triangle of the reference patch $\hat{P} = (0,1)^2$. We begin with configuration B.1 (cf. Figure 11) and choose the degree of freedom belonging to the node x_1. We will show (21) for the triangle T_1. There are two degrees of freedom of V_b that contribute to $\|\nabla v_b\|_{T_1}$. We need to show the existence of a constant $C > 0$ such that

$$(\mathbf{v}_b^1)^2 \leq C\|\sum_{i=1}^{2} \mathbf{v}_b^i \nabla \phi_b^i\|_{T_1}^2 \quad \forall \mathbf{v}_b^1, \mathbf{v}_b^2 \in \mathbb{R}^2 \;\Leftrightarrow\; 1 \leq C\|\nabla\phi_b^1 + \mathbf{v}\nabla\phi_b^2\|_{T_1}^2 \quad \forall \mathbf{v} \in \mathbb{R}. \tag{22}$$

T_1 consists of the nodes $y_0 = (0,0), x_1 = (\frac{1}{2}, \frac{1}{2})$ and $x_2 = (1-r, 0)$ (cf. Figure 11). Using the scaling factor τ_2 defined in (18), it holds for r and s small:

$$\nabla\phi_1|_{T_1} = \begin{pmatrix} 0 \\ 2 \end{pmatrix}, \quad \nabla\phi_2|_{T_1} \approx \tau_2 \begin{pmatrix} 1 \\ -1 \end{pmatrix}, \quad |T_1| \approx \frac{1}{4}$$

and

$$\|\nabla\phi_1\|_{T_1}^2 \approx 1, \quad \|\nabla\phi_2\|_{T_1}^2 \approx \frac{1}{2}\tau_2^2, \quad (\nabla\phi_1, \nabla\phi_2)_{T_1} \approx -\frac{1}{2}\tau_2.$$

For all $\mathbf{v} \in \mathbb{R}$ it holds

$$\begin{aligned} c\|\nabla\phi_1 + \mathbf{v}\nabla\phi_2\|_{T_1}^2 &= c\left(\|\nabla\phi_1\|_{T_1}^2 + 2\mathbf{v}(\nabla\phi_1, \nabla\phi_2)_{T_1} + \mathbf{v}^2\|\nabla\phi_2\|_{T_1}^2\right) \\ &\approx c\left(1 - \tau_2\mathbf{v} + \frac{1}{2}\tau_2^2\mathbf{v}^2\right) = c\left(\frac{1}{2} + \frac{1}{2}\left(1 - \tau_2\mathbf{v}\right)^2\right). \end{aligned}$$

The last term is larger than 1 for $c > 2$ which proves (22).
For the outer nodes (e.g. x_2), we have one of the following two cases (compare (18)):

$$\text{(i) } \tau_2 = \sqrt{r/s} \qquad \text{(ii) } \tau_2 = \sqrt{\max\{r,s\}}$$

In case (i) the contribution from T_4 is dominant for $\|\nabla v_b\|_{\mathcal{N}_i}$. We will show

$$(\mathbf{v}_b^2)^2 \leq C\|\nabla v_b\|_{T_4}^2.$$

T_4 consists of the nodes $x_2 = (1-r, 0), y_1 = (1, 0)$ and $x_3 = (1, s)$. We have

$$\nabla\phi_2|_{T_4} = \tau_2 \begin{pmatrix} 1/r \\ 0 \end{pmatrix}, \quad \nabla\phi_3|_{T_4} = \tau_3 \begin{pmatrix} 0 \\ 1/s \end{pmatrix}, \quad |T_4| = \frac{1}{2}rs$$

and thus

$$c\|\nabla\phi_2 + \mathbf{v}\nabla\phi_3\|_{T_4}^2 = c\|\nabla\phi_2\|_{T_4}^2 + \mathbf{v}^2\|\nabla\phi_3\|_{T_4}^2 \;\geq\; c\|\nabla\phi_2\|_{T_4}^2 = c\frac{\tau_2^2}{r^2}|T_4| = \frac{c}{2} > 1$$

for $c > 2$. In case (ii) we can show

$$(\mathbf{v}_b^2)^2 \leq C\|\nabla v_b\|_{T_1 \cup T_2 \cup T_3}^2$$

using similar basic calculus. In all other cases A, B.2 and B.3, C and D, Assumption (13) can be shown by similar geometric arguments.

References

[1] T. Apel. *Anisotropic finite elements: Local estimates and applications.* Advances in Numerical Mathematics. Teubner, Stuttgart, 1999.

[2] I. Babuška. The finite element method for elliptic equations with discontinuous coefficients. *Computing*, 5:207–213, 1970.

[3] I. Babuška, U. Banarjee, and J.E. Osborn. Generalized finite element methods: Main ideas, results, and perspective. *Int. J. of Comp. Methods*, 1:67–103, 2004.

[4] R.E. Bank and L.R. Scott. On the conditioning of finite element equations with highly refined meshes. *SIAM J. Numer. Anal.*, 26(6):1383–1394, 1989.

[5] S. Basting and R. Prignitz. An interface-fitted subspace projection method for finite element simulations of particulate flows. *Comput. Methods Appl. Mech. Engrg.*, 267:133–149, 2013.

[6] R. Becker and M. Braack. A finite element pressure gradient stabilization for the Stokes equations based on local projections. *Calcolo*, 38(4):173–199, 2001.

[7] R. Becker and R. Rannacher. An optimal control approach to a posteriori error estimation in finite element methods. In A. Iserles, editor, *Acta Numerica 2001*, volume 37, pages 1–225. Cambridge University Press, 2001.

[8] C. Börgers. A triangulation algorithm for fast elliptic solvers based on domain imbedding. *SIAM J. Numer. Anal.*, 27:1187–1196, 1990.

[9] J.H. Bramble and J.T. King. A robust finite element method for nonhomogeneous Dirichlet problems in domains with curved boundaries. *Math. Comp.*, 63:1–17, 1994.

[10] J.H. Bramble and J.T. King. A finite element method for interface problems in domains with smooth boundaries and interfaces. *Advances in Computational Mathematics*, 6:109–138, 1996.

[11] P.G. Ciarlet. Basic error estimates for elliptic problems. In P.G. Ciarlet and J.L. Lions, editors, *Handbook of Numerical Analysis*, volume 2, pages 17–351. Elsevier, 1991.

[12] X. Fang. An isoparametric finite element method for elliptic interface problems with nonhomogeneous jump conditions. *WSEAS Transactions on Mathematics*, 12, 2013.

[13] M. Feistauer and V. Sobotíková. Finite element approximation of nonlinear problems with discontinuous coefficients. *Modél. Math. Anal. Numér.*, 24:457–500, 1990.

[14] A. Hansbo and P. Hansbo. An unfitted finite element method, based on Nitsche's method, for elliptic interface problems. *Comput. Methods Appl. Mech. Engrg.*, 191(47-48):5537–5552, 2002.

[15] A. Hansbo and P. Hansbo. A finite element method for the simulation of strong and weak discontinuities in solid mechanics. *Comput. Methods Appl. Mech. Engrg.*, 193:3523–3540, 2004.

[16] R.J. MacKinnon and G.F. Carey. Treatment of material discontinuities in finite element computations. *Int. J. Numer. Meth. Engrg.*, 24:393–417, 1987.

[17] N. Moës, J. Dolbow, and T. Belytschko. A finite element method for crack growth without remeshing. *Int. J. Numer. Meth. Engrg.*, 46:131–150, 1999.

[18] T. Richter. A fully Eulerian formulation for fluid-structure interactions. *J. Comp. Phys.*, 233:227–240, 2013. http://dx.doi.org/10.1016/j.jcp.2012.08.047.

[19] G.R. Shubin and J.B. Bell. An analysis of grid orientation effect in numerical simulation of miscible displacement. *Comput. Math. Appl. Mech. Eng.*, 47:47–71, 1984.

[20] A.N. Tikhonov and A.A. Samarskii. Homogeneous difference schemes. *USSR Comp. Math. and Math. Phys.*, 1:5–67, 1962.

[21] A. Ženíšek. The finite element method for nonlinear elliptic equations with discontinuous coefficients. *Numer. Math.*, 58:51–77, 1990.

[22] J. Wloka. *Partielle Differentialgleichungen*. Teubner, Stuttgart, 1982.

[23] H. Xie, K. Ito, Z.-L. Li, and J. Toivanen. A finite element method for interface problems with locally modified triangulation. *Contemporary Mathematics*, 466:179–190, 2008.